POLITECNICO
MILANO 1863

DIPARTIMENTO DI MECCANICA

mecc

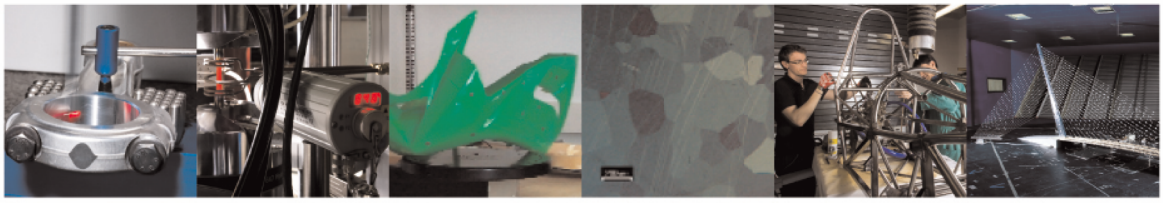

IRLS based inverse methods tailored to volumetric acoustic source mapping

Gianmarco Battista, Gert Herold, Ennes Sarradj, Paolo Castellini, Paolo Chiariotti

This is a post-peer-review, pre-copyedit version of an article published in *Applied Acoustics*.
The final authenticated version is available online at:
http://dx.doi.org/10.1016/j.apacoust.2020.107599

DIPARTIMENTO DI MECCANICA ■ POLITECNICO DI MILANO
via G. La Masa, 1 ■ 20156 Milano ■ EMAIL (PEC): pecmecc@cert.polimi.it
http://www.mecc.polimi.it
Rev. 0

IRLS based inverse methods tailored to volumetric acoustic source mapping

Gianmarco Battista[a], Gert Herold[b], Ennes Sarradj[b], Paolo Castellini[a], Paolo Chiariotti[a,*]

[a] *Università Politecnica delle Marche Via Brecce Bianche 12,60131, Ancona, Italy*
[b] *Technische Universität Berlin, Einsteinufer 25, D-10587 Berlin, Germany*

Abstract

Planar microphone arrays are of common use in acoustic source identification methods, as well as the use of planar calculation grids. Indeed, the assumption is that the planar grid contains all sources of interest. However, this assumption may not be true in several applications and hence return misleading results. One tentative to overcome this issue is to consider three-dimensional surface adhering on the target. Unfortunately, also this choice may not be enough to obtain accurate results in challenging applications like aeroacoustic source mapping, since noise sources are not necessarily located on the surface of the target. This paper aims to analyze the issues and the benefits arising when the calculation grid turns into a volume. Two inverse methods based on Iterative Re-weighted Least Squares (IRLS) and Bayesian Regularization (BR) are formulated: Equivalent Source Method (ESM-IRLS) and Covariance Matrix Fitting (CMF-IRLS). Even though these methods are based on concepts already known in literature, the focus of this paper is on theoretical and algorithmic aspects that make them able to produce accurate volumetric acoustic maps. The methods proposed are applied both on a simulated and an experimental test case. The former is reported to highlight the difference between standard surface mapping and volumetric mapping. The latter reports an application on an airfoil in an open jet. A comparison with the CLEAN-SC approach is reported in both cases to show the performance of the proposed methods with respect to a well-known state of the art algorithm.

1. Introduction

Acoustic source mapping techniques based on microphone arr ays are widely used for localizing noise sources and quantifying their strength. A a matter of fact, however, planar arrays are typically adopted for this purpose, while source mapping is performed on focusing/calculation points laying on planes or

*Corresponding author
Email address: p.chiariotti@univpm.it (Paolo Chiariotti)

3D surfaces that are just supposed to contain all acoustic sources. Indeed, the true location of real sound sources may not lay on these surfaces, thus causing misleading results. This issue often takes place in aeroacoustic noise source identification testing, in which noise sources are very rarely confined on a surface, no matter how complex this could be. For this reasons, volumetric mapping, i.e. mapping on focus/calculation points distributed on a volume rather than on a surface, has raised interest in the aeroacoustic community. However, it is worth noting that such a shift from surface to volume enhances some issues that are typically ignored in the classic surface-based approach. Sarradj [1, 2] analyzed volumetric mapping with direct beamformers and demonstrated that different steering vector formulations (i.e. different spatial filters) are able to provide either correct location or correct level. This limit of beamformers is often masked in surface mapping if the real source is not located on the mapped surface because it produces similar effects. The same study discusses also the need of deconvolving beamforming maps, due to poor spatial resolution in radial direction from array centre. Fast deconvolution techniques such as Orthogonal Beamforming [3] and CLEAN-SC [4] are suggested due to the huge problems size. Indeed, these two approaches are characterized by a reasonable computation time. The use of DAMAS (or one of its extension) [5, 6, 7] is theoretically possible but discouraged due to its huge computational cost. Another possible choice for volumetric mapping is the use of inverse methods, e.g. Generalized Inverse Beamforming (GIB) [8], Equivalent Source Method (ESM) [9], Covariance Matrix Fitting (CMF) [6] or Bayesian Approach to sound source reconstruction (BA) [10]. Padois et al. compared the performances of different techniques (CB,GIB,DAMAS and CLEAN-SC) in three-dimensional mapping and also studied the effect of using multiple planar arrays simultaneously [11, 12]. Porteous et al. [13] described how to deal with volumetric mapping with CB and CLEAN-SC using two orthogonally aligned planar arrays looking at the same sources. Ning et al. [14] used Compressed sensing techniques to face three-dimensional source mapping problem. Battista et al. [15, 16] studied how to deal with inverse methods for volumetric aeroacoustic mapping in wind tunnels using one or two planar arrays.

The focus of this work is to identify the main issues and the benefits lying behind volumetric acoustic imaging. Two formulations of inverse methods based on Iteratively Re-Weighted Least Squares (IRLS) tailored to volumetric mapping (ESM-IRLS and CMF-IRLS) are proposed. The problem is faced here considering the use of a single planar array, given the wide availability and use of such a configuration. However, the issues linked to the volumetric approach and the methods proposed are still valid when different array configurations (e.g. multiple microphone arrays) are adopted. A simulated test case has been used to perform comparison between 2D/3D imaging and show how a small offset between mapping surface and actual source position deteriorates the quality of the reconstruction in terms of localization/quantification accuracy. Then, volumetric maps obtained on an airfoil in open jet are shown to demonstrate the efficacy of the approach on a real test case. In both cases, a comparison

with the CLEAN-SC deconvolution approach is performed.

2. The volumetric acoustic inverse problem

To better understand inverse methods is mandatory to start from direct formulation of acoustic propagation from a set of elementary sources (e.g. monopoles, dipoles, plane waves etc.) to receiver locations. Indeed, the direct acoustic problem formulation relies on the Wave Superposition Method [17] which states that the acoustic field, generated by a complex radiator, can be reproduced as a superposition of fields caused by a set of simpler sources enclosed within the radiator. In frequency domain, the discrete direct source-receiver propagation problem is linear and can be written, for each frequency, as:

$$\mathbf{G}\mathbf{q} = \mathbf{p}\,, \tag{1}$$

where $\mathbf{q} \in \mathbb{C}^{N\times 1}$ is the vector of N complex source coefficients, $\mathbf{p} \in \mathbb{C}^{M\times 1}$ is a vector containing acoustic complex pressures at microphone locations and $\mathbf{G} \in \mathbb{C}^{M\times N}$ is the acoustic transfer matrix. The calculation of $\mathbf{p}$ for a given $\mathbf{q}$ and $\mathbf{G}$ identifies the direct acoustic problem, which is well-determined and has unique solution. Contrarily, the inverse acoustic problem aims to retrieve the source distribution $\mathbf{q}$ from measurement at microphone locations $\mathbf{p}$, given a direct propagator $\mathbf{G}$. This problem results to be ill-posed in the Hadamard sense [18, 19], i.e. existence, uniqueness and stability of the solution are not guaranteed. The inverse problem formulation can be as well expressed as a linear transformation:

$$\hat{\mathbf{q}} = \mathbf{H}\mathbf{p}\,, \tag{2}$$

where $\hat{\mathbf{q}}$ is the solution for a particular inverse operator $\mathbf{H} \in \mathbb{C}^{N\times M}$. When the acoustic field is stationary, the former problem can be rearranged in terms of auto- and cross- power spectra averaged over several observations:

$$\mathbf{G}\mathbf{Q}\mathbf{G}^H = \mathbf{P}\,, \tag{3}$$

where the superscript ^{H} stands for the complex conjugate transpose operator. The matrix $\mathbf{P} = \langle \mathbf{p}\mathbf{p}^H \rangle$ is the Cross Spectral Matrix (CSM) of pressure at microphone locations and $\mathbf{Q} = \langle \mathbf{q}\mathbf{q}^H \rangle$ is the CSM of sources strengths ($\langle\cdot\rangle$ is the average operator over time blocks). Using the quadratic form, the solution of the inverse problem can be obtained as

$$\hat{\mathbf{Q}} = \mathbf{H}\mathbf{P}\mathbf{H}^H\,. \tag{4}$$

The source auto-powers are on the main diagonal of $\hat{\mathbf{Q}}$ and are indicated throughout the paper with $\mathrm{diag}(\hat{\mathbf{Q}})$ (intended as column vector) or Q_{nn} (element-wise).

The inverse operator can be formulated in different ways, depending on the selected solution method, assumptions and a priori information considered. A complete review about different inverse operators is provided by Leclere et al. in

[20]. Beamforming methods [21] consider each potential source separately, thus having a scalar inverse problem. The main advantage of inverse methods with respect to classic direct beamforming approach is that all sources are considered together, thus leading to better results in terms of source strength quantification and in presence of multiple correlated/uncorrelated acoustic sources. However, since the number of potential sources is usually much greater than the number of microphones, the problem is generally under determined and different approaches can be adopted to obtain a particular solution that optimally satisfies a condition.

2.1. Issues in volumetric acoustic mapping

The application of acoustic mapping methods to an extended spatial domain is straightforward, while obtaining accurate and useful results requires a deeper analysis of the problem. When it comes to volumetric acoustic imaging, three critical issues have to considered:

- potential sources located at very different distances from the array;
- poor spatial resolution in the radial direction from the array centre;
- increase of number of potential sources with no contribution to the acoustic field.

These problems are also present in classic plane/surface mapping. However, their effects are dramatically enhanced in volumetric imaging, therefore, they must be carefully understood and addressed to avoid getting misleading results.

As far as the first issue is concerned, potential sources near the array need less energy to produce a given pressure on receivers with respect to farther sources. Acoustic imaging methods, which rely on energy minimization of source field, may tend to locate acoustic sources closer to the array than their actual location. This problem is common to 2D and 3D applications, but it gets more relevant when it comes to volumetric mapping. A simple strategy to overcome this problem is to balance the energy needed by each potential source to generate the same pressure at microphones locations.

The second item of the list is a well known issue in acoustic imaging: the radial direction from the array centre suffers of poor spatial resolution, with respect to the lateral directions, unless the microphone arrangement encloses the source. This aspect can be an issue even when multiple planar arrays are used together and it gets worse as the source distance from the array centre increases. In order to understand how this effect influences the results, it is useful to recall what happens in conventional beamforming mapping (the reader can also refer to the examples presented in [1, 21]). Indeed, even a point source produces, in a volumetric map, a beam whose axis links the array centre and

the source location. As the wavelength and source-array distance increase, the cross-section of the beam increases as well. In this context, beamforming maps allow to distinguish different sources only when they are angularly spaced with respect to the array centre, otherwise the beams would be superposed and hardly distinguishable, even if the sources are at different distances from the array.

The last issue relates to the increase of the number of potential sources that may lay within a volume rather than on a surface. In fact, few thousands potential sources ($10^3 \div 10^4$) might be involved when distributed on a surface, while hundred thousands potential sources ($10^4 \div 10^5$) might lay within a volume. This implies theoretical and practical issues. The increase in the number of unknowns makes the problem heavily under-determined. The latter is related to the computational demand of techniques, that must be affordable and reasonable even with this huge problem size.

Deconvolution of volumetric beamforming maps with CLEAN-SC is the best choice in terms of speed, since its computational demand is only a bit greater than a conventional frequency domain beamformer. As for DAMAS-based deconvolution techniques, the computational demand is often prohibitive when it comes to such a high number of calculation points, since DAMAS-based deconvolution approaches require calculation of all PSFs and then the solution of an inverse problem (generally $N \times N$). Inverse methods have been chosen in this work since they return the whole source distribution at once and can successfully deal with correlated/uncorrelated sources. In addition, they provide accurate results in a reasonable computation time even with hundred thousands potential sources. Despite this advantage, the ill-posedness and the ill-conditioning of the inverse problem are two issues that sill need to tackled. Indeed, these two aspects are enhanced by the huge problem size. In the next section, all the aspects discussed above are addressed in the formulation of an approach tailored to volumetric mapping.

3. Tailored IRLS approach for solving sparse approximation of volumetric source field

Many IRLS approaches for acoustic imaging are available in literature, such as GIB [8], ESM [9], Compressive ESM [22] and sparse acoustical holography from iterated Bayesian Focusing (IBF) [23]. The one proposed here does not differ from the others for theoretical basis, but it adopts several strategies needed to tackle the issues discussed in the previous section in order to obtain accurate solutions in volumetric context.

3.1. Problem definition and sparsity constraint

The main assumption adopted is sparsity of the solution. Indeed, despite the growth of the problem size when addressing volumetric imaging, the actual sound sources can be still approximated with "few" equivalent sources. This

can be seen as a priori information helping in compensating the lack of information that is intrinsic of acoustic inverse problems. When sparsity constraint is enforced, the basis in which this happens is crucial, since the hypothesis cannot be true in some source representations. A sparsity constraint on the sought solution can be enforced by minimizing the following cost function

$$\hat{\mathbf{q}}(\eta^2, p) = \arg\min_{\mathbf{q}} \left(\|\mathbf{G}\mathbf{q} - \mathbf{p}\|_2^2 + \eta^2 \|\mathbf{q}\|_p^p \right) \tag{5}$$

where $\| \cdot \|_p^p$ is the L_p-norm of a vector. The main three terms of this cost function are:

- $\|\mathbf{q}\|_p^p$ is the L_p-norm of of the solution, where $0 \leq p \leq 2$. Adjusting the exponent of the norm different amount of sparsity in the solution is achieved.
- $\|\mathbf{G}\mathbf{q} - \mathbf{p}\|_2^2$ is the fitting error. This term represents the fidelity of the solution with respect to measured data.
- η^2 is the regularization parameter and controls the trade-off between the two terms above. Its estimation is difficult because it depends on problem formulation and data. This is probably the most critical aspect of the method.

The strongest sparsity constraint is enforced setting $p = 0$, while $p = 2$ means no sparsity. Intermediate values (e.g. in descending order from $p = 2$) cause an increase in the level of sparsity. For $p < 1$ this turns in a more difficult non-convex optimization problem, while for $p \geq 1$ the optimization problem is convex. Therefore, $p = 1$ is the strongest sparsity that can be enforced with a convex optimization problem. Unfortunately, there is no analytic solution to L_p minimization problem, but for $p = 2$. In fact, this is the case of Tikhonov Regularization [24] or a particular case of the Bayesian Approach to Sound Source Reconstruction (BA) [10]. Both approaches make it possible to have an analytical solution to the following problem:

$$\hat{\mathbf{q}}(\eta^2, \mathbf{W}) = \arg\min_{\mathbf{q}} \left(\|\mathbf{G}\mathbf{q} - \mathbf{p}\|_2^2 + \eta^2 \|\mathbf{W}\mathbf{q}\|_2^2 \right) \tag{6}$$

where the square invertible matrix $\mathbf{W}$ is used to introduce a priori information about the solution. This aspect is particularly well explained in BA. The inverse operator that results from this approach is:

$$\mathbf{H} = \mathbf{W}^{-2}\mathbf{G}^H(\mathbf{G}\mathbf{W}^{-2}\mathbf{G}^H + \eta^2\mathbf{I})^{-1} \,. \tag{7}$$

The Iteratively Reweighted Least Squares (IRLS) [25, 26] can be used for obtaining an approximation of the solution of Eq. 5. This approach is based on the analytical solution of Eq. 6 and on the assumption

$$\|\mathbf{q}\|_p^p = \sum_{n=1}^{N} |q_n|^p = \sum_{n=1}^{N} w_{nn}^2 |q_n|^2 = \|\mathbf{W}\mathbf{q}\|_2^2 \,. \tag{8}$$

The matrix $\mathbf{W}$ is square, real and diagonal and the set of weights w_{nn} depends on the result of the previous iteration, according to the following expression:

$$w_{nn}^{(it)} = \left| \hat{q}_n^{(it-1)} \right|^{\frac{(p-2)}{2}} \tag{9}$$

where it stands for the current iteration. Basically, for each iteration a regularized Weighted Least-Squares problem is solved, exploiting the solution of the previous iteration to find a better approximation of the solution of Eq. 5.

3.2. Direct acoustic operator

The choice of the direct acoustic propagator is an important step since it defines both the investigation zone (i.e. location of potential sources) and the source model. Only monopoles are considered as potential source models, but the method is general enough to be transferred also to different types of elementary sources. Once defined the investigation zone and the source models, the discretization of the investigation zone can be done adopting either a uniform grid or a more generic distribution of potential sources. Unlike direct beamformers, the solution of an inverse formulation is influenced, and even more in a volumetric approach, by the definition of the investigation zone and by its discretization. In fact, the energy required by each potential source to produce a certain pressure at microphone locations should be properly balanced. This can be done using a strength-to-pressure acoustic transfer function in combination with a weighting strategy, as suggested by Pereira et al. [27]. A similar concept is explained in [13]. If only monopoles are considered as potential sources, the acoustic propagator and the weights can be calculated as:

$$G_{mn} = \frac{\mathrm{e}^{-\mathrm{j}kr_{mn}}}{4\pi r_{mn}} \quad , \quad w_{nn} = \frac{1}{r_{0n}} \tag{10}$$

where k is the wavenumber. The terms r_{mn} represent the propagation distances between microphones (m) and the potential sources (n). The weights w_{nn} are calculated as the reciprocal of terms r_{0n} that are the propagation distances between the reference point "0" and the location of potential sources. The reference point is usually set at the array centre, but it can be chosen arbitrarily, avoiding the coincidence with a potential source location. The weighting matrix $\mathbf{W}$ hosting the weighting coefficients w_{nn} is diagonal. The elements of the weighted direct operator $\mathbf{G}\mathbf{W}^{-1}$ becomes:

$$G_{mn} w_{nn}^{-1} = \frac{r_{0n}}{r_{mn}} \frac{\mathrm{e}^{-\mathrm{j}kr_{mn}}}{4\pi} \, . \tag{11}$$

An alternative choice is the pressure-to-pressure acoustic transfer function formulation [28], which embeds compensation of source distances. For monopoles, the propagator can be written in the following form:

$$G_{mn} = \frac{r_{0n}}{r_{mn}} \mathrm{e}^{-\mathrm{j}k(r_{mn}-r_{0n})} \, . \tag{12}$$

This propagator relates the pressure in the reference point "0", generated by a monopole located in n, to the pressure induced on microphone m. This is the formulation adopted in this paper to solve inverse problems since the balance is straightforward. Solutions returned by the two formulations of propagator are in different physical units (volume acceleration of each source or pressure induced by a monopole at the reference point). However, solutions are equivalent if expressed in the same unit.

3.3. IRLS procedure

The IRLS procedure can be formalized with the following expression:

$$\hat{\mathbf{q}}^{(it)} = F\left(\hat{\mathbf{q}}^{(it-1)}, \mathbf{W}^{(it)}, \eta^{2\,(it)}, \mathbf{G}^{(it)}, \mathbf{p}, p\right) , \tag{13}$$

where the function F is given by Eq. 6 and the superscript (it) addresses those quantities that are updated at each iteration. The main steps of the algorithm are listed hereafter. Two inputs must be set at first:

- p: order of the L_p-norm that sets the strength of sparsity constraint;
- $\mathbf{W}_0$: weighting matrix that introduce arbitrary a priori information on the source field. This term is named Aperture Function in BA.

The IRLS procedure adopted is the following:

1. Set the weighting matrix $\mathbf{W}^{(it)}$ for the current iteration:

$$\mathbf{W}^{(it)} = \mathbf{W}_0\, \mathbf{W}_{sp}^{(it)} . \tag{14}$$

   The matrix $\mathbf{W}_{sp}^{(it)}$ is used to force the sparsity (Eq. 9) and $\mathbf{W}_{sp}^{(1)} = \mathbf{I}$.
2. Estimate the regularization parameter $\eta^{2\,(it)}$ for the current iteration.
3. Calculate the solution $\hat{\mathbf{q}}^{(it)}$ using the inverse operator of Eq. 7.
4. Discard potential sources that do not contribute significantly to the acoustic field.
5. Evaluate a convergence criterion: if not fulfilled go back to step 1 otherwise stop.

This iterative procedure represents a fixed-point scheme for Eq. 5 that converges to its minimum. In case of convex problems ($p \geq 1$) the minimum is unique and global, while multiple local minima may also be present for non-convex problems ($0 \leq p < 1$). Influence of p is studied in [29]. From Bayesian point of view, this method can be seen as an Expectation-Maximization algorithm that converges to a Maximum A Posteriori (MAP) estimation of the source field [30].

As for step 1, both matrices are normalized such that $\|\mathbf{W}_0\|_\infty = \|\mathbf{W}_{sp}^{(it)}\|_\infty = 1$ and then multiplied to give them the same weight. The resulting matrix $\mathbf{W}^{(it)}$

is normalized such that trace($\mathbf{W}^{(it)}$) = N. The matrix $\mathbf{W}_0$ is constant for all iterations and can be used to introduce arbitrary information about the source distributions. This helps in reducing the lack of information in the inverse problem, while an identity matrix means no a priori information introduced.

Step 2, which addresses the estimation of the amount of regularization, can be considered as the most critical step. The parameter η^2 must be correctly estimated at each iteration to guarantee the stability of result. Empirical Bayesian Regularization (BR) is adopted since it has been demonstrated to outperform many other regularization techniques. The interested reader might refer to [31] for a deeper insight into this topic. In this work, the MAP estimate of the regularization parameter is adopted. The MAP estimate aims at minimizing the following cost function with respect to η^2:

$$\mathbf{J}_{MAP}(\eta^2) = \sum_{k=1}^{M} \ln(s_{kk}^2 + \eta^2) + (M-2)\ln\left(\frac{1}{M}\sum_{k=1}^{M}\frac{|y_k|^2}{s_k^2+\eta^2}\right). \qquad (15)$$

The calculation of this cost function requires the Singular Value Decomposition of the matrix $\mathbf{G}\mathbf{W}^{-1} = \mathbf{U}\mathbf{S}\mathbf{V}^H$; the term s_{kk} refers to the k-th singular value (diagonal elements of $\mathbf{S}$) while $y_k = \mathbf{u}_k^H\mathbf{p}$ refers to the k-th Fourier coefficient ($\mathbf{u}_k$ is the k-th column of $\mathbf{U}$). Even though other strategies can be utilized to estimate the regularization parameter, one should remember that in IRLS under-regularized solutions in any iteration may compromise the final result. On the other hand, over-regularized solution may produce two effects: a loss of details in the final acoustic map, since weaker sources may be suppressed, and under-estimation of source strength.

Step 3 refers to the application of Eq. 7, where $\mathbf{G}^{(it)}$, $\mathbf{W}^{(it)}$ and $\eta^{2\,(it)}$ are used. Step 4 requires deeper attention. In fact, weights in Eq. 9 imply that source coefficients must be different from zero. This is avoided by applying an amplitude threshold to the current solution $\hat{\mathbf{q}}^{(it)}$ in order to discard sources that do not contribute significantly to the acoustic field. These sources are discarded from the calculation and are set to 0 in the final solution. The set of indexes n of sources to discard at each iteration is found using the following criterion:

$$\left\{ n : 10\log_{10}\left(\frac{|\hat{q}_n|^{(it)}}{\|\hat{\mathbf{q}}^{(it)}\|_\infty}\right) < THR_{dB} \right\}. \qquad (16)$$

The threshold THR_{dB} should be low enough to avoid any influence on the result. Indeed, big negative values are recommended. All the results showed in this paper are obtained with the THR_{dB} threshold set to -100 dB. This value makes it possible to quickly discard several potential sources, thus speeding up the calculations. The propagation matrix $\mathbf{G}^{(it)}$ is then updated removing columns associated to the sources discarded. The same happens to the weighting matrix $\mathbf{W}^{(it)}$.

The convergence of the solution at each iteration is checked on Step 5. The

rate of convergence depends on p and $\mathbf{W}_0$, but it is also highly-data dependent. A convergence criterion should guarantee uniformity of results even in different conditions. A good convergence criterion should ensure that changes of solution are getting smaller both spatially and in terms of amplitude. In [32], a convergence criterion (C1) is suggested:

$$\varepsilon^{(it)} = 10 \log_{10} \left(MSR \right) \tag{17}$$

$$MSR^{(it)} = \left\langle \left| \hat{q}_n^{(it)} / \hat{q}_n^{(it-1)} \right| \right\rangle \tag{18}$$

where MSR stands for *Mean Source Ratio* and the operator $\langle \cdot \rangle$ refers to spatial average. This criterion requires that source amplitudes remain almost unaltered in the last 2 iterations to stop the algorithm. If potential sources are discarded in two consecutive iterations, MSR is calculated using only those common to both solutions. The value $\varepsilon^{(it)}$ approaches asymptotically to 0 dB from negative values. Some fluctuations may happen due to sudden changes in two consecutive solutions, especially when $p < 1$, due to discarding of sources. To increase the robustness to this issue, in [15, 33] a slightly different criterion (C2) is proposed, which is also used in this paper:

$$\varepsilon^{(it)} = 10 \log_{10} \left(MSR^{(it)} - \left| \Delta(MSR)^{(it)} \right| - \left| \Delta^2(MSR)^{(it)} \right| \right) \tag{19}$$

where the operators $\Delta(\cdot)$ and $\Delta^2(\cdot)$ are the backward finite differences of first and second order. This criterion can be evaluated only for $it > 2$ because of the second order finite difference in the formula. The additional terms prevent the convergence in case of eventual variations that may occur in consecutive IRLS solutions. This criterion requires that variations in the solution are small over the last 3 iterations. Negative values, that may result in the argument to the logarithm, mean that convergence is not met. This criterion tends to Eq. 17 when MSR changes smoothly during consecutive iterations, hence it should be considered as a safety condition. In this work, the convergence of the solution is accepted when $\varepsilon^{(it)} \geq -0.1$ dB using C2.

3.4. ESM-IRLS

The Equivalent Source Method described in this work aims at finding a solution to the inverse acoustic problem using the linear formulation, therefore starting from Eq. 1. Each element of the discrete propagator $\mathbf{G}$ is calculated using Eq. 12. In this case, a sparse approximation of the source field is recovered considering only monopoles. However, the method is general enough to consider also other elementary source representations (e.g. dipole, quadrupole, etc.). Suzuki [8] suggested to decompose CSM in coherent source components and solve an inverse problem for each of them. The Eigenmode Decomposition (ED) relies on the property of CSM of being Hermitian and non-negative definite, thus having the following decomposition:

$$\mathbf{P} = \mathbf{E}_{vec} \, \mathbf{E}_{val} \, \mathbf{E}_{vec}^H \, , \tag{20}$$

where $\mathbf{E}_{val}$ is a diagonal matrix with all real positive eigenvalues and $\mathbf{E}_{vec}$ is a unitary matrix with M orthonormal eigenvectors. The CSM diagonal is kept, otherwise some eigenvalues may result negative. Once the eigenvalues are sorted in descending order, it is possible to define the eigenmode $\mathbf{e}_m$ as the eigenvector including its amplitude

$$\mathbf{e}_m = \sqrt{e_{val,m}}\, \mathbf{e}_{vec,m} \qquad m = 1, \ldots, M \tag{21}$$

where $\mathbf{e}_{vec,m}$ is the m-th eigenvector and $e_{val,m}$ is the corresponding eigenvalue. Each eigenmode represents a coherent signal across the microphones, under an orthogonality constraint. An inverse problem is solved for each eigenmode, according to

$$\mathbf{G}\mathbf{q}_i = \mathbf{e}_i \qquad i = 1, \ldots, C \tag{22}$$

where $C \leq M$ is the number of most energetic eigenmodes that are considered as relevant.

It should be highlighted, however, that applying an inverse problem to each eigenmode of the CSM will necessarily destroy the sparsity of the solution in the general setting. Indeed, the eigenvalue decomposition is a L2 minimization, which is contradictory with the recovery of sparsity. If eigenmodes are processed independently, neither IRLS nor any other L_p-norm minimzer, $p < 2$, will be able to efficiently restore sparsity. This will be kept only if eigenmodes are extracted jointly or even afterwards the IRLS procedure. When the latter condition holds, the total map can be calculated as a sum of the source powers associated to the most energetic C eigenmodes for each point of the map:

$$\hat{Q}_{nn} = \sum_{i=1}^{C} |\hat{q}_{n,i}|^2 \qquad n = 1, \ldots, N\,. \tag{23}$$

Other CSM decompositions can be adopted with ESM-IRLS, an example of this can be found in [15, 16], where CLEAN-SC is exploited as a tool to extract single coherent source components from CSM. In this paper ESM-IRLS is applied to Eq. 3 with no decomposition step.

3.5. CMF-IRLS

The Covariance Matrix Fitting approach, described in [6, 34], aims at finding the source field that best approximates pressure CSM of microphones. Sources are assumed to be uncorrelated in the standard CMF formulation. This implies null off-diagonal terms in the $\mathbf{Q}$ matrix. Consequently, Eq. 3 can be rearranged as a standard linear system:

$$\mathbf{P_c} = \mathbf{G_c}\ \mathrm{diag}(\mathbf{Q}) \tag{24}$$

where $\mathbf{P_c}$ is the microphone CSM reshaped in column vector form and the matrix $\mathbf{G_c}$ is computed using the elements of the direct operator $\mathbf{G}$. The explicit form

of Eq. 24 is:

$$\begin{bmatrix} \langle p_1 p_1^* \rangle \\ \langle p_1 p_2^* \rangle \\ \vdots \\ \langle p_i p_j^* \rangle \\ \vdots \\ \langle p_M p_M^* \rangle \end{bmatrix} = \begin{bmatrix} G_{11}G_{11}^* & \dots & G_{1n}G_{1n}^* & \dots & G_{1N}G_{1N}^* \\ G_{11}G_{21}^* & \dots & G_{1n}G_{2n}^* & \dots & G_{1N}G_{2N}^* \\ \vdots & \dots & \vdots & \dots & \vdots \\ G_{i1}G_{j1}^* & \dots & G_{in}G_{jn}^* & \dots & G_{iN}G_{jN}^* \\ \vdots & \dots & \vdots & \dots & \vdots \\ G_{M1}G_{M1}^* & \dots & G_{Mn}G_{Mn}^* & \dots & G_{MN}G_{MN}^* \end{bmatrix} \begin{bmatrix} Q_{11} \\ Q_{22} \\ \vdots \\ Q_{nn} \\ \vdots \\ Q_{NN} \end{bmatrix} \tag{25}$$

where the indices $i, j = 1, \dots, M$ are used for microphones and $n = 1, \dots, N$ is the index of potential sources and the term $\langle \cdot \rangle$ stands for the averaging operator. Each term $G_{in}G_{jn}^*$ represents the cross-spectrum between microphones i and j, when the n-th source with unitary power is active. The system has N unknowns and M^2 equations. However, the number of independent equations reduces to $M_c = M^2 - M$ when Diagonal Removal is exploited to exclude self-noise on microphones. This is the formulation used in this work. Even though the source model is the same of ESM-IRLS (monopoles), the problem is formulated using different bases ($\mathbf{G_c}$ instead of $\mathbf{G}$), therefore, this is important when the sparsity condition is enforced.

The Q_{nn} elements represent source auto-powers, hence they must be real and non-negative. The "realness" of the solution is guaranteed from a mathematical point of view by the structure of the matrices. Algorithms as Non-negative Least Square could be used to comply with this condition. However, also if using the IRLS procedure described in this paper, the positivity constraint on solution is applied at each iteration discarding source having negative power, in addition to the other discarding strategy described in Section 3.3. In this way, source having non-physical negative power are forced to 0 as in the Gauss-Seidel procedure of DAMAS.

4. Results

4.1. Simulated data

The first test case is the Analytical Benchmark 8, available at [35]. This dataset represents a simulation of measurements in an open jet wind tunnel with a round jet. Noise sources are three monopoles emitting uncorrelated white noise with the same level. Simulated setup is depicted in Fig. 1. The 64 microphones array is situated above the volume and has an aperture of $D = 1.5$ m. The flow is along x-axis direction and the sound propagation through the flow field is calculated using the *Acoular* OpenJet environment [36]. The nozzle diameter is 0.5 m, the jet flow speed is 0.2 Mach and speed of sound is 343 m/s.

	x	y	z
Source 1	0.10	0.00	-0.50
Source 2	0.10	0.12	-0.50
Source 3	0.10	0.24	-0.50
Nozzle centre	-0.60	0.00	-0.50

Table 1: Setup coordinates (m)

	x (m)	y (m)	z (m)
Plane 1			-0.50
Plane 2	[-0.50 , +0.50]	[-0.50 , +0.50]	-0.48
Plane 3			-0.52
Volume			[-0.20 , -1.00]

Table 2: Regions of interest for the simulated test case. The values in the square brackets indicates the extension of the region.

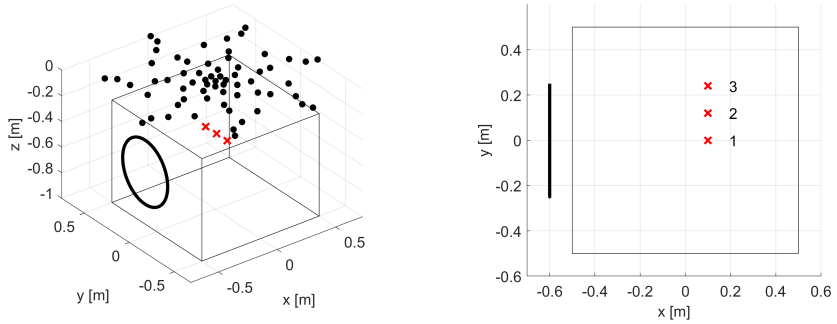

(a) (b)

Figure 1: Simulated measurement setup. Black circle is the nozzle. Black dots are the microphone locations. Red crosses are source locations. (a) Side view. (b) Top view.

A comparative analysis between 2D and 3D mapping is provided in this section. Table 2 reports the coordinates of the planes and volume mapped and all are discretized with regular grid of monopoles with 2 cm step. Each plane has 2.601 potential sources while the volume has 106.641 potential sources. Planes 2 and 3 have an offset of 2 cm from the exact source positions. Three mapping methods are applied to this test case: ESM-IRLS, CMF-IRLS and CLEAN-SC. The latter is applied using a loop-gain $\varphi = 0.6$.

It has been checked that the use of further components does not affect the solution neither in terms of localization nor in terms of quantification of the sources. The maximum sparsity constraint is enforced setting $p = 0$, while uniform aperture function has been used. This choice tends to produce the

best quantification results when adopting the inverse methods addressed in this paper. Source spectra reconstructed are obtained by integrating maps over a spherical volume of 6 cm radius centred in the exact source location. The integral is calculated summing the auto-powers of equivalent sources. Reconstructed source spectra are depicted as ratio, in terms of source strength, between the exact source spectrum and the one obtained from the maps. The frequency range of analysis goes from 2 kHz to 9 kHz, that corresponds to the range $He = 8.5 \div 38.3$, where He is the Helmholtz number calculated as the ratio of array diameter and wavelength. As rule of thumb, all mapping methods tend to have troubles to provide accurate maps when $He < 8$ in presence of multiple sources, therefore, this low range of He is not considered here.

Figures from 2 to 4 shows the comparison of volumetric maps (Volume) with planar ones (Plane 1). In this case, acoustic sources are contained in the regions of interest (ROI), while in Fig. 5 to 7, the planes used to produce the acoustic maps are 2 cm above (Plane 2) or below (Plane 3) the actual source locations. This produces apparently no artifacts with CLEAN-SC, while slightly deteriorates the quality of maps obtained with ESM and CMF. It is worth noticing that all methods are able to correctly return the exact source locations in volumetric maps. Figure 8 depicts the errors in source spectra reconstruction obtained with all mapping techniques tested in this work, when different regions of interest are used. All methods clearly shows that the offset of Plane 2 and 3 with respect to source location produces the underestimation of source strengths. This effect is particularly evident with CLEAN-SC and CMF, from about 5 kHz towards higher frequencies, but even ESM confirm this trend despite its instability in source strength quantification. Figure 9 compares the source quantification error obtained with all methods on volumetric maps. The major instability in source quantification of ESM-IRLS, with respect to the other two methods, can be partially attributed to the assumption of uncorrelated sources made for CMF-IRLS and CLEAN-SC. In case of correlated and distributed sources however, it is expected that CLEAN-SC performance gets worse. Experimental test case in the next section is an example of this.

When it comes to processing time, the following data can be reported (CPU: Intel Xeon E5-2630 v4 @ 2.20 GHz, RAM: 128 GB @ 2400 MHz). For 2D calculations, CLEAN-SC took about 0.11 seconds, CMF-IRLS 6.67 seconds and ESM-IRLS 1.9 seconds. For inverse method a non negligible increase of processing time is experienced when planes "out of focus" are considered. In this condition, CMF-IRLS took 7.45 seconds while ESM-IRLS 2.55 seconds. Instead for 3D calculations, CLEAN-SC took 5.50 seconds, CMF-IRLS 210.56 seconds and ESM-IRLS 18.61 seconds. It is worth to remember that with ESM an inverse problem for each eigenmode is solved, while with CMF only one on the whole CSM.

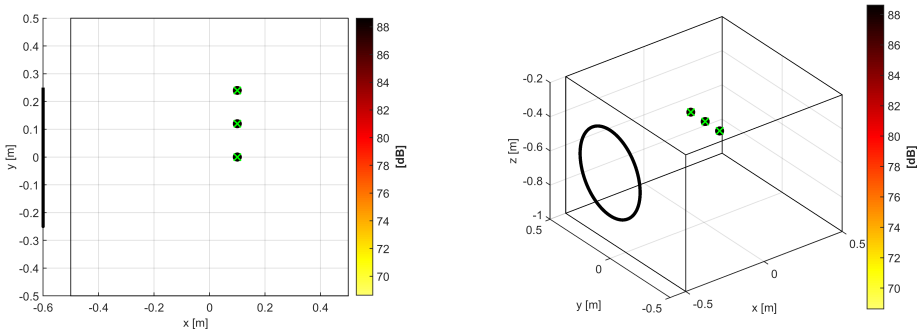

(a) (b)

Figure 2: 2D vs 3D mapping with CLEAN-SC, 8 kHz 1/3-octave band. (a) Plane 1. (b) Volume.

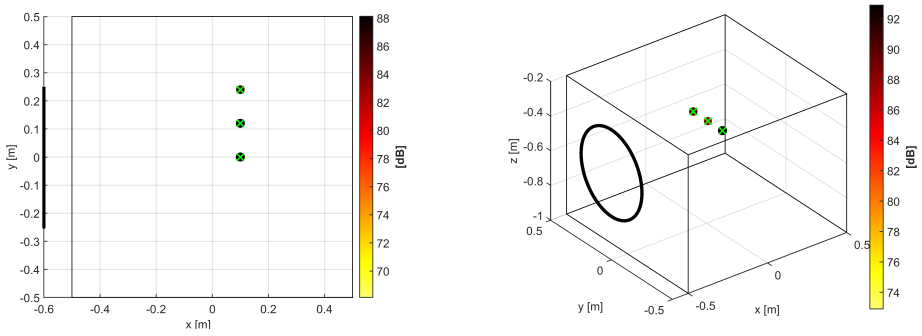

(a) (b)

Figure 3: 2D vs 3D mapping with ESM-IRLS, 8 kHz 1/3-octave band. (a) Plane 1. (b) Volume.

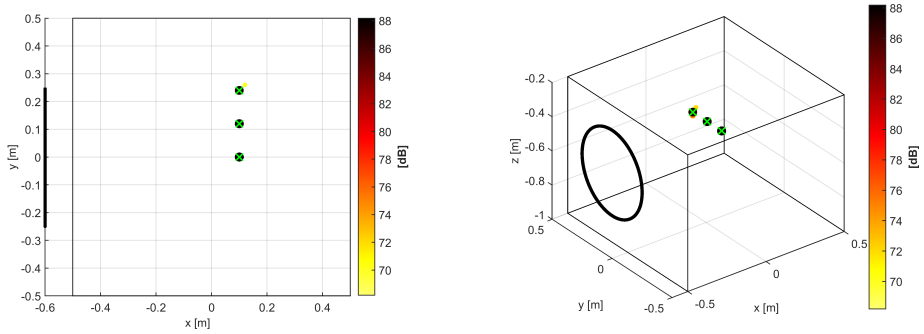

(a) (b)

Figure 4: 2D vs 3D mapping with CMF-IRLS, 8 kHz 1/3-octave band. (a) Plane 1. (b) Volume.

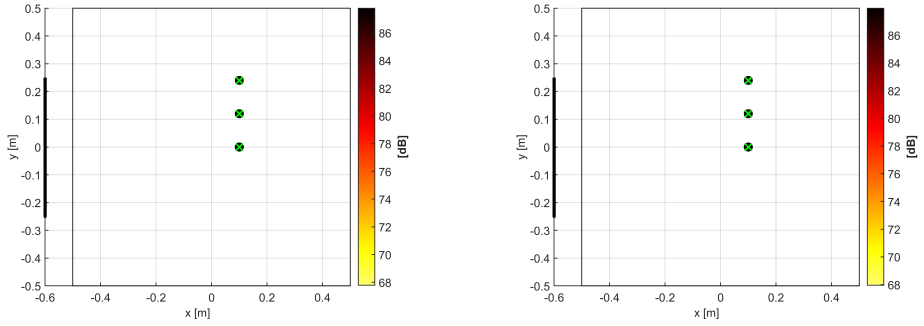

(a) (b)

Figure 5: 2D mapping with CLEAN-SC, 8 kHz 1/3-octave band. (a) Plane 2. (b) Plane 3.

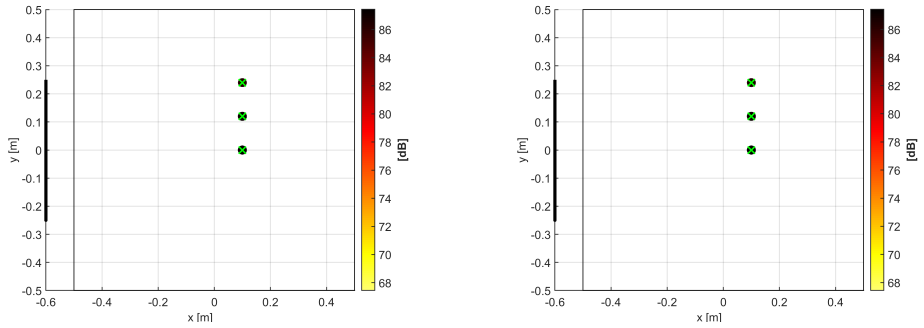

(a) (b)

Figure 6: 2D mapping with ESM-IRLS, 8 kHz 1/3-octave band. (a) Plane 2. (b) Plane 3.

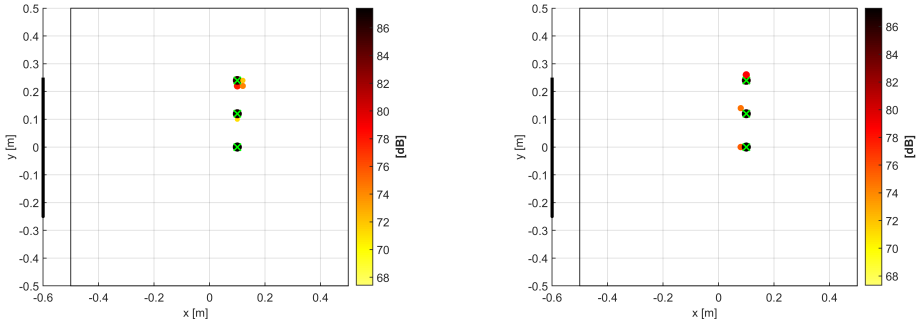

Figure 7: 2D mapping with CMF-IRLS, 8 kHz 1/3-octave band. (a) Plane 2. (b) Plane 3.

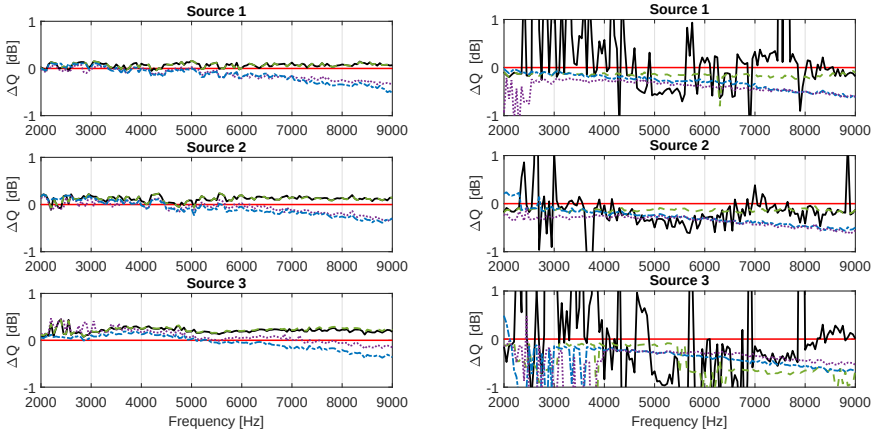

(a)

(b)

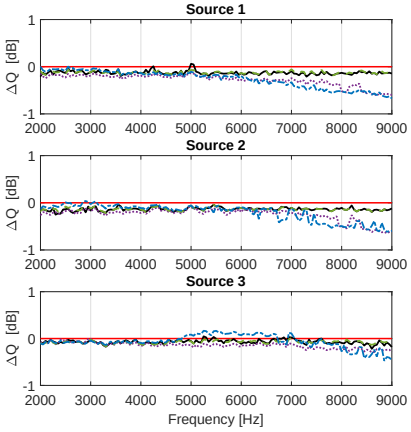

(c)

Figure 8: Error of reconstructed source spectra with different regions of interest. Black solid line: Volume. Green dashed line: Plane 1. Purple dotted line: Plane 2. Blue dot-dashed line: Plane 3. (a) CLEAN-SC. (b) ESM-IRLS. (c) CMF-IRLS.

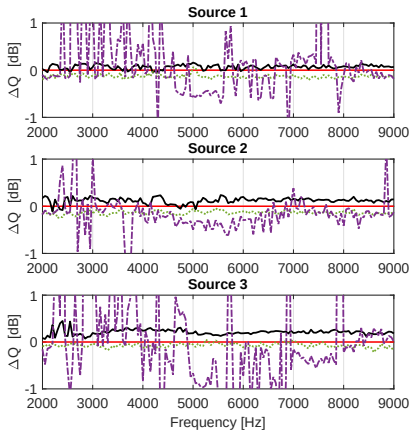

Figure 9: Error of reconstructed source spectra with different methods in volumetric source mapping. Black solid line: CLEANSC. Green dotted line: CMF-IRLS. Purple dot-dashed line: ESM-IRLS.

4.2. Experimental data

The second test case is a real experiment conducted in the aeroacoustic wind tunnel at Brandenburg University of Technology [37]. A NACA 0012 airfoil is positioned in an open jet of diameter 0.2 m and core velocity 50 m/s. The airfoil has a span of 0.28 m and a chord length of 0.25 m. The boundary layer tripping was realized with a 2.5 mm anti-slip tape applied at 10% of the chord both on the suction and the pressure side. The array used has 56 microphones and a diameter $D = 1.3$ m; it was placed 0.715 m above the airfoil. Figure 10 shows the position of the airfoil and the nozzle. Data were sampled at 51200 samples/s and the CSM is estimated averaging 4000 blocks of 1024 samples (overlap 50%) using Hanning window. The frequency resolution obtained is 50 Hz. Also in this test case the sound propagation through the flow field is calculated using *Acoular* OpenJet environment, in order to get the actual propagation distances. As for the acoustic propagator is concerned, standard free field pressure-to-pressure formulation is used. No masking effect due to the solid airfoil is currently considered. Authors are developing solutions to tackle this issue, but this will be discussed in future works.

The target volume for delivering acoustic maps is the outer region depicted in Fig. 10. This volume is discretized in a regular grid of 2 cm spacing. Since monopoles are considered, this discretization turns into 60.516 potential sources. The inner region is exploited to define an arbitrary aperture function. All coordinates of both regions are available in Tab. 3. An arbitrary aperture function is introduced in the processing of experimental data to reduce the influence of disturbing sources outside the mapped region. The aperture function is equal to 1 for each point inside the inner region and has values that decrease to 0 towards the edges of the outer region. Figure 11 depicts the weights profile, used to calculate the aperture function, which are obtained similarly to a Cosine-

Tapered window (or Tukey window). The weight of each point is calculated as the product of Wx, Wy and Wz, depending on its coordinates, and these values are used to define the diagonal of the inverse of $\mathbf{W}_0$, which is the actual weighting matrix used in calculations.

Results referring to the 1/3-octave bands with central frequencies 4 kHz and 8kHz, which correspond to $He \approx 13.5 \div 16.7$ and $He \approx 26.8 \div 33.5$, are reported hereafter. CLEAN-SC produces quite clear maps, even though the sources identified, both at the leading and trailing edges, are too spatially concentrated with respect to the distribution suggested by the physics of the phenomenon. The adoption of $\varphi < 1$ could help in mitigating the risk to alter the shape of spatially distributed sources. ESM-IRLS seems to respect the spatial extension of the noise sources expected. This is true also for the CMF-IRLS approach, despite this latter method seems to preserve the spatial distribution of source in a less precise way.

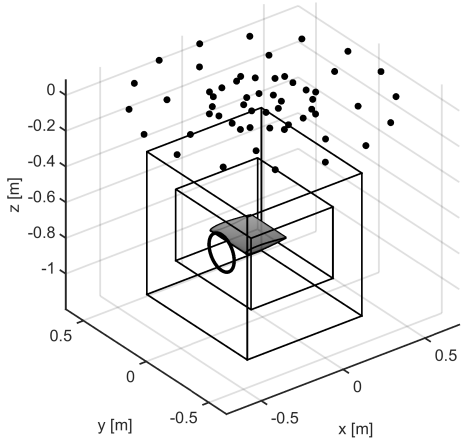

Figure 10: Measurement setup. In gray the airfoil NACA 0012. The black circle is the nozzle of the open jet. Black dots are the microphone locations.

	x (m)	y (m)	z (m)
Outer region	[-0.400 , +0.300]	[-0.400 , +0.400]	[-1.115 , -0.315]
Inner region	[-0.300 , +0.200]	[-0.300 , +0.300]	[-0.915 , -0.515]

Table 3: Regions of interest for the experimental test case. The values in the square brackets indicates the extension of the region.

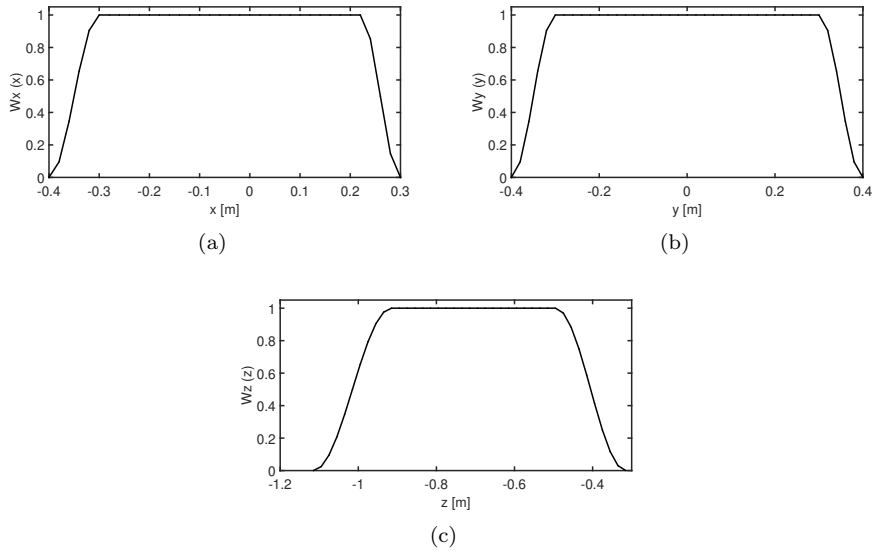

Figure 11: Weights profile used to create the Aperture Function. (a) Profile along x axis. (b) Profile along y axis. (c) Profile along z axis.

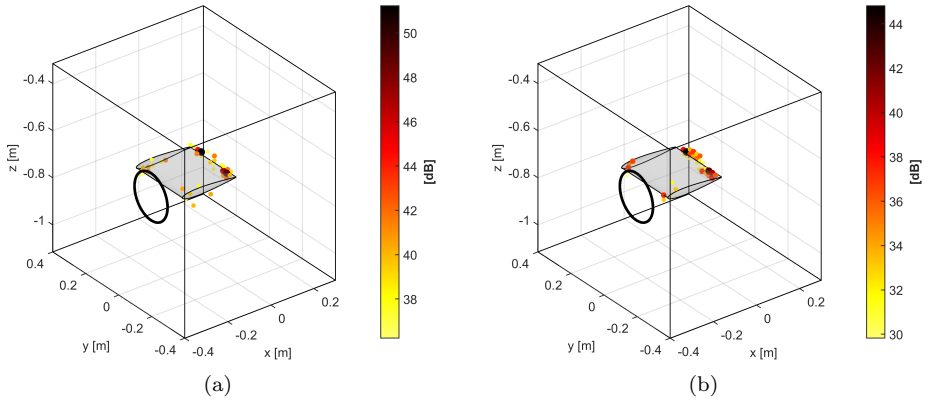

Figure 12: Volumetric 3D maps on airfoil NACA 0012 in open jet with CLEAN-SC. (a) 4 kHz 1/3-octave band. (b) 8 kHz 1/3-octave band.

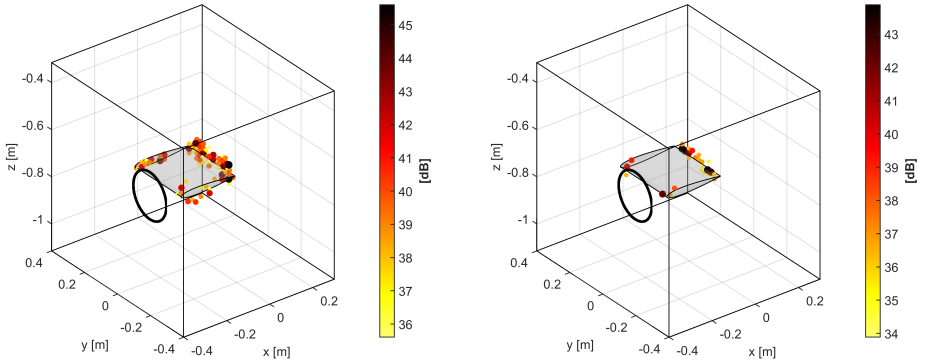

Figure 13: Volumetric 3D maps on airfoil NACA 0012 in open jet with ESM-IRLS. (a) 4 kHz 1/3-octave band. (b) 8 kHz 1/3-octave band.

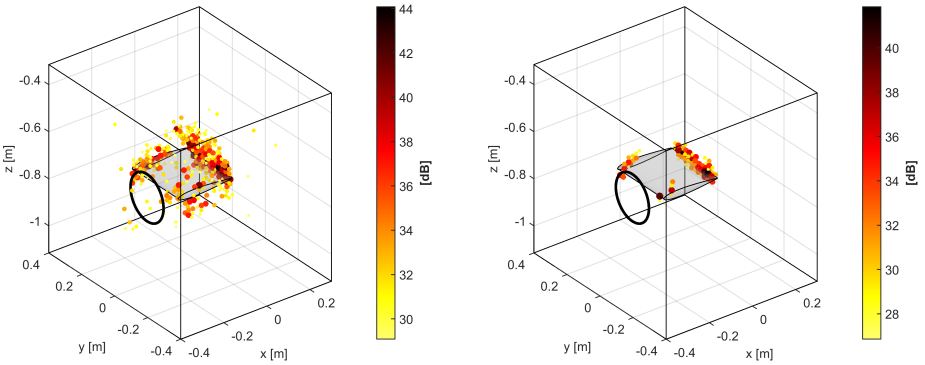

Figure 14: Volumetric 3D maps on airfoil NACA 0012 in open jet with CMF-IRLS. (a) 4 kHz 1/3-octave band. (b) 8 kHz 1/3-octave band.

5. Conclusions

A study on three-dimensional volumetric mapping with inverse methods has been presented in this paper. The use of a single planar array makes source localization and quantification a very difficult tasks, because additional issues must be faced with respect to standard acoustic imaging performed on grids that lay on surfaces. A tailored IRLS approach has been discussed for solving sparse approximation of source field in volumetric context. Two inverse methods have been proposed: ESM-IRLS and CMF-IRLS. These two methods have been compared with CLEAN-SC both on simulated and experimental test cases. It has been shown that standard approach of surface mapping produces errors in source spectra reconstruction, when the surface does not contains the real sources. Moreover, some artifacts may be present in acoustic maps. Despite the higher complexity, volumetric three-dimensional approach demonstrated to bring advantages in terms of localization and quantification. The application on experimental data of an airfoil in open jet showed several sources out of the chord plane and the airfoil surface. A positive aspect of the volumetric approach is that it does not require any additional hardware or any sort of modification to typical measurement setup, therefore it can be applied also to measurement data already acquired for standard acoustic mapping.

References

[1] E. Sarradj, Three-dimensional acoustic source mapping with different beamforming steering vector formulations, Advances in Acoustics and Vibration 2012 (292695) (2012) 1–12. doi:10.1155/2012/292695.

[2] E. Sarradj, Three-dimensional acoustic source mapping, in: 4th Bebec, 2012.

[3] E. Sarradj, C. Schulze, A. Zeibig, Identification of Noise Source Mechanisms using Orthogonal Beamforming, in: Noise and Vibration: Emerging Methods, 2005.

[4] P. Sijtsma, Clean based on spatial source coherence, International Journal of Aeroacoustics 6 (4) (2007) 357–374.
URL http://dx.doi.org/10.1260/147547207783359459

[5] T. F. Brooks, W. M. Humphreys, Jr, A deconvolution approach for the mapping of acoustic sources (DAMAS) determined from phased microphone array, Journal of Sound and Vibration 294 (4-5) (2006) 856–879. doi:10.1016/j.jsv.2005.12.046.

[6] T. Yardibi, J. Li, P. Stoica, L. N. Cattafesta, Sparsity constrained deconvolution approaches for acoustic source mapping, The Journal of the Acoustical Society of America 123 (5) (2008) 2631–2642. doi:http://dx.doi.org/10.1121/1.2896754.

URL http://scitation.aip.org/content/asa/journal/jasa/123/5/10.1121/1.2896754

[7] T. F. Brooks, W. M. Humphreys, Jr, Extension of DAMAS Phased Array Processing for Spatial Coherence Determination (DAMAS-C), in: 12th AIAA/CEAS Aeroacoustics Conference, Cambridge, Massachusetts, May 8-10, 2006, 2006.

[8] T. Suzuki, L1 generalized inverse beam-forming algorithm resolving coherent/incoherent, distributed and multipole sources, Journal of Sound and Vibration 330 (2011) 5835–5851. doi:10.1016/j.jsv.2011.05.021.

[9] A. Pereira, Acoustic imaging in enclosed spaces, Ph.D. thesis, INSA de Lyon (2014).

[10] J. Antoni, A bayesian approach to sound source reconstruction: Optimal basis, regularization, and focusing, The Journal of the Acoustical Society of America 131 (4) (2012) 2873–2890. doi:10.1121/1.3685484.

[11] T. Padois, A. Berry, Two and three-dimensional sound source localization with beamforming and several deconvolution techniques, Acta Acustica united with Acustica 103 (3) (2017) 392–400. doi:10.3813/aaa.919069.

[12] T. Padois, O. Robin, A. Berry, 3d source localization in a closed wind-tunnel using microphone arrays, in: 19th AIAA/CEAS Aeroacoustics Conference, American Institute of Aeronautics and Astronautics (AIAA), 2013. doi:10.2514/6.2013-2213.

[13] R. Porteous, Z. Prime, C. Doolan, D. Moreau, V. Valeau, Three-dimensional beamforming of dipolar aeroacoustic sources, Journal of Sound and Vibration 355 (2015) 117–134. doi:10.1016/j.jsv.2015.06.030.

[14] F. Ning, J. Wei, L. Qiu, H. Shi, X. Li, Three-dimensional acoustic imaging with planar microphone arrays and compressive sensing, Journal of Sound and Vibration 380 (2016) 112–128. doi:10.1016/j.jsv.2016.06.009.

[15] G. Battista, P. Chiariotti, M. Martarelli, P. Castellini, Inverse methods in aeroacoustic three-dimensional volumetric noise source localization and quantification, Journal of Sound and Vibration 473 (2020) 115208. doi:https://doi.org/10.1016/j.jsv.2020.115208.
URL http://www.sciencedirect.com/science/article/pii/S0022460X20300390

[16] Gianmarco Battista, Paolo Chiariotti, Milena Martarelli, Paolo Castellini, Inverse methods in aeroacoustic three-dimensional volumetric noise source localization, in: Proceedings of ISMA-USD 2018, 2018.

[17] G. H. Koopmann, L. Song, J. B. Fahnline, A method for computing acoustic fields based on the principle of wave superposition, The Journal of the Acoustical Society of America 86 (6) (1989) 2433–2438. doi:10.1121/1.398450.

[18] J. Hadamard, Sur les problèmes aux dérivés partielles et leur signification physique,(On the partial derivative problems and their physical meaning), Princeton University Bulletin 13 (1902) 49–52.

[19] P. C. Hansen, Rank-deficient and discrete ill-posed problems, SIAM Monographs on Mathematical Modeling and Computation, Society for Industrial and Applied Mathematics (SIAM), Philadelphia, PA, 1998, numerical aspects of linear inversion.

[20] Q. Leclère, A. Pereira, C. Bailly, J. Antoni, C. Picard, A unified formalism for acoustic imaging based on microphone array measurements, International Journal of Aeroacoustics 16 (4-5) (2017) 431–456. doi:10.1177/1475472x17718883.

[21] P. Chiariotti, M. Martarelli, P. Castellini, Acoustic beamforming for noise source localization – reviews, methodology and applications, Mechanical Systems and Signal Processing 120 (2019) 422–448. doi:10.1016/j.ymssp.2018.09.019.

[22] E. Fernandez-Grande, A. Xenaki, P. Gerstoft, A sparse equivalent source method for near-field acoustic holography, The Journal of the Acoustical Society of America 141 (1) (2017) 532–542. doi:10.1121/1.4974047.

[23] J. Antoni, T. L. Magueresse, Q. Leclère, P. Simard, Sparse acoustical holography from iterated bayesian focusing, Journal of Sound and Vibration 446 (2019) 289–325. doi:10.1016/j.jsv.2019.01.001.

[24] A. N. Tikhonov, Solution of incorrectly formulated problems and the regularization method, Soviet Math. Dokl. 4 (1963) 1035–1038.

[25] R. Chartrand, W. Yin, Iteratively reweighted algorithms for compressive sensing, in: 2008 IEEE International Conference on Acoustics, Speech and Signal Processing, IEEE, 2008. doi:10.1109/icassp.2008.4518498.

[26] I. Daubechies, R. DeVore, M. Fornasier, C. S. Güntürk, Iteratively reweighted least squares minimization for sparse recovery, Communications on Pure and Applied Mathematics 63 (1) (2010) 1–38. doi:10.1002/cpa.20303.

[27] A. Pereira, Q. Leclère, Improving the Equivalent Source Method for noise source identification in enclosed spaces, in: 18th International Congress on Sound and Vibration (ICSV 18), Brazil, 2011, p. R31.
URL https://hal.archives-ouvertes.fr/hal-01006201

[28] G. Herold, E. Sarradj, T. Geyer, Covariance matrix fitting for aeroacoustic application, in: Fortschritte der Akustik - DAGA, 2013.

[29] Q. Leclere, A. Pereira, J. Antoni, Une approche bayésienne de la parcimonie pour l'identification de sources acoustiques, in: Congrès Français d'Acoustique, Poitiers, France, 2014, pp. –.
URL https://hal.archives-ouvertes.fr/hal-01006192

[30] F. Champagnat, J. Idier, A connection between half-quadratic criteria and EM algorithms, IEEE Signal Processing Letters 11 (9) (2004) 709–712. doi:10.1109/lsp.2004.833511.

[31] A. Pereira, J. Antoni, Q. Leclère, Empirical bayesian regularization of the inverse acoustic problem, Applied Acoustics 97 (2015) 11–29. doi:10.1016/j.apacoust.2015.03.008.

[32] B. Oudompheng, A. Pereira, C. Picard, Q. Leclère, B. Nicolas, A theoretical and experimental comparison of the iterative equivalent source method and the generalized inverse beamforming, in: 5th BeBec, 2014.
URL http://bebec.eu/Downloads/BeBeC2014/Papers/BeBeC-2014-12.pdf

[33] G. Battista, P. Chiariotti, G. Herold, E. Sarradj, P. Castellini, Inverse methods for three-dimensional acoustic mapping with a single planar array, in: Proceedings of the 7th Berlin Beamforming Conference, 2018.

[34] G. Herold, E. Sarradj, T. Geyer, Covariance matrix fitting for aeroacoustic application, in: Fortschritte der Akustik - AIA-DAGA 2013, 2014, pp. 1926 – 1928.

[35] Benchmarking array analysis methods (2018).
URL https://www.b-tu.de/fg-akustik/lehre/aktuelles/arraybenchmark

[36] Acoular acoustic testing and source mapping software (2018).
URL http://www.acoular.org

[37] G. Herold, T. F. Geyer, E. Sarradj, Comparison of inverse deconvolution algorithms for high-resolution aeroacoustic source characterization, in: 23rd AIAA/CEAS Aeroacoustics Conference, American Institute of Aeronautics and Astronautics, 2017. doi:10.2514/6.2017-4177.